

## SYNTHESIS OF MANGANESE DOPED ZINC SULPHIDE NANOCRYSTALLINE POWDERS BY WET-CHEMICAL SYNTHESIS ROUTE

A.-I. CADIȘ<sup>a\*</sup>, E.-J. POPOVICI<sup>a</sup>, E. BICA<sup>a</sup>, I. PERHAIȚA<sup>a</sup>,  
L. BARBU-TUDORAN<sup>b</sup>, E. INDREA<sup>c</sup>, L. SILAGHI-DUMITRESCU<sup>d</sup>

<sup>a</sup> "Raluca Ripan" Institute for Research in Chemistry, Babes- Bolyai University, 30 Fântânele, 400294 Cluj-Napoca, Romania

<sup>b</sup> Electronic Microscopy Centre, Babes-Bolyai University, 5-7 Clinicilor, 400006 Cluj-Napoca, Romania

<sup>c</sup> National Institute for Research and Development of Isotopic and Molecular Technologies, 65-103 Donath, 400293 Cluj-Napoca, Romania

<sup>d</sup> Faculty of Chemistry and Chemical Engineering, Babes- Bolyai University, 11 Arany Janos, 400028 Cluj-Napoca, Romania

Manganese-doped zinc sulphide nanocrystalline powders with photoluminescence properties were synthesised by wet-chemical synthesis route WCS *via* the reagent simultaneous addition technique SimAdd. In order to control both the morpo-structural and optical properties of ZnS:Mn<sup>2+</sup> nanoparticles, precipitation was carried out, from sodium sulphide and zinc-manganese acetate mixture with variable manganese amount, in methanol medium containing methacrylic acid, sodium dodecylsulphate or cetyl-trimethyl-ammonium bromide as organic additives. Samples were characterized by ICP-optical emission spectroscopy, thermogravimetric analysis, infrared absorption spectroscopy, photoluminescence spectroscopy, transmission electron microscopy and X-ray diffraction. A correlation between the preparation conditions and the physical-chemical properties, photoluminescence and morpo-structural characteristics of ZnS:Mn<sup>2+</sup> powders were established.

(Received August 11, 2011; accepted October 3, 2011)

*Keywords:* Chalcogenides; Precipitation; Luminescence; Nanostructures;

### 1. Introduction

Nanomaterials and nanostructures play an important role in various application fields such as energy sources, environment, health and medical treatments. The physical and chemical properties of nanomaterials are exceptionally dependent on the particle size or morphology. Due to their unique properties, which lead to new and exciting applications, nanomaterials are increasingly gaining the attention of the scientific community but also the public [1].

Nanoparticles and nanostructured II-VI semiconductors account for the most investigated materials, due to their special properties [2-4]. Zinc sulphide-based materials have attracted increasing interest with respect to their applications in optoelectronics [5], photocatalysis [6], targeted drug delivery [7], biosensors [8], light emitting diodes [9] etc. Through controlling the size and the doping of zinc sulphide (ZnS) particles with transition metal [6] or rare-earth ions [10], different materials with new properties and uses could be obtained.

Manganese-doped zinc sulphide (ZnS:Mn<sup>2+</sup>) nanocrystals could exhibit orange luminescence with high fluorescence quantum efficiency under the interband excitation of the host crystal by UV light [11]. This spectacular result illustrates that nanocrystalline ZnS:Mn<sup>2+</sup> system may be considered a new class of luminescent material of interest for the manufacture of optic and optoelectronic devices i.e. displays, lighting equipments and lasers [12].

---

\* Corresponding author: cadisadi@chem.ubbcluj.ro

Zinc sulphide nanoparticles (NP-ZnS) can be obtained in many ways such as solid-state reaction [10], organometallic route [11], low temperature thermolysis [13], wet chemical route [14], microwave irradiation [15] and solution-phase thermal decomposition route [16]. The studies revealed that the ZnS particle dimensions and photoluminescent (PL) properties depend strongly on the specific preparation method and the applied experimental conditions. The development of new synthesis routes and techniques is the target of the latest researches, with the purpose of achieving a good control of NP-ZnS properties.

The most popular method for the preparation of luminescent zinc sulphide is the wet-chemical synthesis-WCS route or co-precipitation method performed with or without organic additives that act as surfactants i.e., cysteine or serine [17], cetyl-pyridinium chloride or cetyl-trimethyl-ammonium bromide [18], sodium dodecylsulphate [19] or as passivating agents i.e. 2-mercaptoethanol [6], poly(vinylpyrrolidone) [20], sodium polyphosphate [21], polyvinyl alcohol [22] or methacrylic acid [23].

The WCS route is an inexpensive synthesis method and has a large-scale-production potential [24]. Usually, nanocrystalline ZnS:Mn<sup>2+</sup> powders are obtained by adding the precipitants one-into-another *via* the reagent sequential addition technique, abbreviated SeqAdd [14, 25]. Our previous studies referring to micro-phosphors synthesis revealed that powders with well-controlled optical and morpho-structural properties can be obtained by WCS route *via* the reagent simultaneous addition technique, abbreviated SimAdd [26-28].

This study continues our researches devoted to the synthesis of luminescent, nanostructured ZnS particles and layers [25, 29-31]. The goal of the paper is to illustrate that, the WCS-SimAdd route can be successfully used to obtain homogeneous Mn-doped ZnS nanocrystalline powders with PL properties. Our preliminary researches revealed that, the dispersion capability of ZnS:Mn<sup>2+</sup> powders is low when they are separated from aqueous medium [32]. Moreover, the powder quality can be improved when SimAdd synthesis is performed in the presence of methacrylic acid as passivating agent [33].

New physical and chemical aspects referring to the synthesis of ZnS:Mn<sup>2+</sup> nanoparticles using the reagent simultaneous addition technique are reported in the present paper. In order to control the particle morphology and size and to improve the powders quality, the precipitation was carried out in a medium with low dielectric constant (e.g. methanol), in the presence of three different acting organic additives namely methacrylic acid – MAA as passivating agent, sodium dodecylsulphate – SDS as cationic surfactant and cetyl-trimethyl-ammonium bromide – CTAB as anionic surfactant. The investigation is focussed on the influence of the Mn-concentration and organic additives on the photoluminescence and morpho-structural properties of ZnS:Mn<sup>2+</sup> powders obtained *via* WCS-SimAdd route. General physical-chemical characteristics (based on thermogravimetric analysis, ICP-OES analysis of the actual Mn-amount from powders, and FTIR spectroscopy) as well as photoluminescence (determined by emission and excitation measurements) or morpho-structural properties (evaluated by X-ray diffraction and transmission electron microscopy) are taken into consideration in relation with the synthesis of luminescent ZnS:Mn<sup>2+</sup> nanocrystals. It has to be mentioned, that excepting our preliminary studies, no other investigations referring to the properties of ZnS:Mn<sup>2+</sup> powders prepared by WCS-SimAdd route have been reported so far.

## 2. Experimental

Manganese doped zinc sulphide powders were prepared by WCS-SimAdd, at room temperature, in methanol-based medium, from 1M aqueous solution of Zn-Mn acetate and sodium sulphide, respectively. In this purpose, equal volumes (100 ml) of Zn-Mn acetate mixture and Na<sub>2</sub>S solutions were simultaneously added, with controlled flow capacity, under continuous and strong stirring, into 400 ml methanol containing 0.050 mol organic reagent i.e. 11.0 g/l MAA, 36.6 g/l SDS and 46.2 g/l CTAB, respectively. The manganese amount from Zn-Mn acetate mixture was varied between 0 mol% and 16.0 mol% from the total metal amount. The resulting ZnS:Mn<sup>2+</sup> powders were cautiously washed with methanol, centrifuged, and finally dried at 80°C, under vacuum.

Two samples series were precipitated without additives, using variable manganese amounts i.e. 0 mol% (C35), 1.6 mol% (C34), 5.0 mol% (C33), 8.0 mol% (C36) and 16.0 mol% (C32) and, correspondingly, with the same manganese amount (8.0 mol%) and different organic additives i.e. MAA (C59), CTAB (C39) and SDS (C38). With the exception of C59 powder, all ZnS:Mn<sup>2+</sup> samples were obtained at pH= 6.3-6.5, using a local precipitant concentration of  $7.5\text{-}5.0 \times 10^{-5}$  mol/L. The MAA-sample (C59) was prepared at relative lower pH (5.7), due to the acidity induced by the additive.

ZnS:Mn<sup>2+</sup> powders were synthesised from Zn(CH<sub>3</sub>COO)<sub>2</sub> x 2H<sub>2</sub>O (p.a., Merck), Mn(CH<sub>2</sub>COO)<sub>2</sub> x 4H<sub>2</sub>O (for synthesis, Merck), Na<sub>2</sub>S x 9H<sub>2</sub>O (min. 98%, Sigma), methanol (p.a., ing. Petr Svec Penta), cetyl-trimethyl-ammonium bromide (min. 99%, Sigma), sodium dodecylsulphate (p.a. Loba Feinchemie) and methacrylic acid (purum, Fluka). Before use, zinc/manganese acetate and sodium sulphide solutions were purified by cross-precipitation.

The infrared absorption spectra (FT-IR) of ZnS:Mn<sup>2+</sup> samples were recorded with a THERMO SCIENTIFIC NICOLET™ 6700 FT-IR spectrometer (KBr pellets). Photoluminescence emission (PL) and photoluminescence excitation (PLE) spectra were registered with JASCO FP-6500 spectrofluorimeter Wavell, equipped with PMT R928 photomultiplier (glass filter WG 320-ReichmannFeinoptik). The most intense sample prepared without additive (C36) was used as internal standard ( $I_{em} = 100\%$ ). The thermogravimetric analysis (TGA) was carried out with a METTLER-TOLEDO TGA/SDTA851 instrument, under 30 ml/min nitrogen flow, with a heating rate of 5°C/min (63.0- 65.5 mg sample). The transmission electron microscopy (TEM) was performed with JEM JEOL 1010 microscope, with an accelerating voltage of 20 kV. The powders were dispersed in ethanol, with a standard ultrasound bath, and deposited on 400 meshes copper grid, which was coated with carbon film. X-ray diffraction (XRD) measurements were performed using a BRUKER D8 Advance X-ray diffractometer, working at 40 kV and 40 mA and the goniometer was equipped with a germanium monochromator in the incident beam. The X-ray diffraction patterns were collected in a step-scanning mode with steps of  $\Delta 2\theta = 0.01^\circ$  using Cu K $\alpha$ 1 radiation ( $\lambda = 1.54056 \text{ \AA}$ ). Corundum powder was used as standard for instrument broadening correction. The chemical analysis of ZnS:Mn<sup>2+</sup> powders was carried out from hydrochloric solutions, by inductively coupled plasma optical emission spectroscopy (ICP-OES), using a PERKIN ELMER OPTIMA 2100 DV spectrometer. The manganese and zinc detection was made at 257.61 nm (detection limit 1  $\mu\text{g/L}$ ) and 206.20 nm (detection limit 0.4  $\mu\text{g/L}$ ), respectively.

### 3. Results and discussion

The goal of our studies was to obtain and characterise luminescent manganese doped zinc sulphide nanocrystals *via* WCS-SimAdd route. In this purpose, ZnS:Mn<sup>2+</sup> powders were obtained by the simultaneous precipitation of MnS and ZnS, from methanol-based medium, with or without organic additives i.e. methacrylic acid as passivating agent, sodium dodecylsulphate as anionic surfactant and cetyl-trimethyl-ammonium bromide as cationic surfactant.

The influence of both the manganese concentration and organic additive on the general physical-chemical, photoluminescent and morpho-structural properties of ZnS:Mn<sup>2+</sup> powders was investigated.

#### 3.1. General physical-chemical properties

The precipitation conditions determine the actual composition of ZnS:Mn<sup>2+</sup> powders, by influencing both the MnS/ZnS balance and the amount of adsorbed anionic/molecular species.

The actual Mn concentrations as well as the water and organics amount from ZnS powders were evaluated with ICP-OES and TGA analysis (Table 1). The Mn co-precipitation level is estimated on the basis of the ratio between the actual and the calculated (theoretic) manganese concentration. The total weight-loss at 1100°C and the partial values for three temperature domains were calculated on the basis of TG curves. The onset point, above 900°C was used to evaluate ZnS sublimation point of ZnS-based powders

The actual Mn-concentration in ZnS powders represents less than 10% from the theoretical value. This can be explained by the fact that, the precipitation rate of the two metallic

sulphides is different as a consequence of the large difference between their solubility products, namely  $2.5 \times 10^{-22}$  for cubic ZnS form, and  $2.5 \times 10^{-10}$  for amorphous MnS form [34].

Table 1. Manganese concentration ( $Mn \times 100/(Mn+Zn)$ ) and thermogravimetric analysis data for  $ZnS:Mn^{2+}$  powders obtained in different precipitation conditions.

Code	Organic additive	Mn-concentration (mol%)		Mn co-precipitation level (%)	TGA weight-loss (wt%)				Sublimation point (°C)
		theoretic	actual		temperature domain (°C)			Total	
					20-200	200-900	900-1100		
C32	-	16.0	0.94	5.88	-6.2	-8.8	-5.2	-20.2	1042
C33	-	5.0	0.19	3.80	-6.5	-8.8	-4.7	-20.0	1045
C34	-	1.6	0.05	3.13	-6.3	-9.6	-5.5	-21.4	1043
C35	-	0.0	0.00	0.00	-6.2	-9.8	-5.6	-21.6	1045
C36	-	8.0	0.25	3.13	-6.0	-10.1	-5.3	-21.4	1042
C38	SDS	8.0	0.28	3.50	-5.7	-11.3	-5.8	-22.8	1039
C39	CTAB	8.0	0.05	0.63	-6.5	-9.9	-5.9	-22.3	1044
C59	MAA	8.0	0.74	9.25	-5.3	-10.1	-5.8	-21.2	1037

This study reveals that, the Mn doping level in ZnS powders is dependent on both the organic additive used as particle size regulator and the initial manganese concentration. Among the powders prepared without organic additive, the sample with the largest Mn-amount (C32) yields the highest co-precipitation level (~5.9%). The organic additive MAA and the cationic surfactant CTAB yield the highest (~9.3%) and, correspondingly, the lowest (~0.6%) co-precipitation level. It is obvious that both additives interfere in the Zn-Mn co-precipitation process, by increasing and respectively decreasing the Mn precipitation rate.

The thermal behaviour of  $ZnS:Mn^{2+}$  powders is dependent on the precipitation conditions (Table 1; Fig.1). All samples show three major endothermic stages that can be associated with: a) removal of the physically adsorbed water (below 200°C); b) removal of organic ions absorbed from the precipitation medium (between 200 and 900°C); c) volatilization/sublimation of zinc sulphide under the cumulative effect of temperature and nitrogen flow (above 900°C). The samples tendency toward volatilization, evaluated by the weight-loss and the sublimation point/onset temperature above 900°C, is dependent on the  $ZnS:Mn^{2+}$  powder dispersion and particle dimensions.

The weight-loss values of samples C32-C36 prepared without additives, with variable Mn-amount are similar. According to TGA data, the water and the organics content is 6.0-6.5%, and correspondingly 8.8-10.1%, and the amount of volatilised ZnS is 4.7-5.6%; the point of sublimation is in 1042-1045°C domain. For samples prepared with organic additives (C38, C39, C59), the weight-loss above 200°C domain is higher (15.8-17.1%) than for the sample prepared with no additive (15.4%). As for the sublimation point, this one is relatively low for MAA- and SDS-powders (1037; 1039°C) as compared with the no additive sample, probably due to the relative smaller particle dimensions. On the contrary, the sublimation point of CTAB-sample is a little higher, thus suggesting that ZnS particles are larger.

The influence of the organic additive on the differential thermogravimetric (DTG) curves is illustrated in Fig. 1. One can note that, in the 200-900°C range, the organics removal takes place either in three steps (C36, C38 and C59) or in four steps (C38).

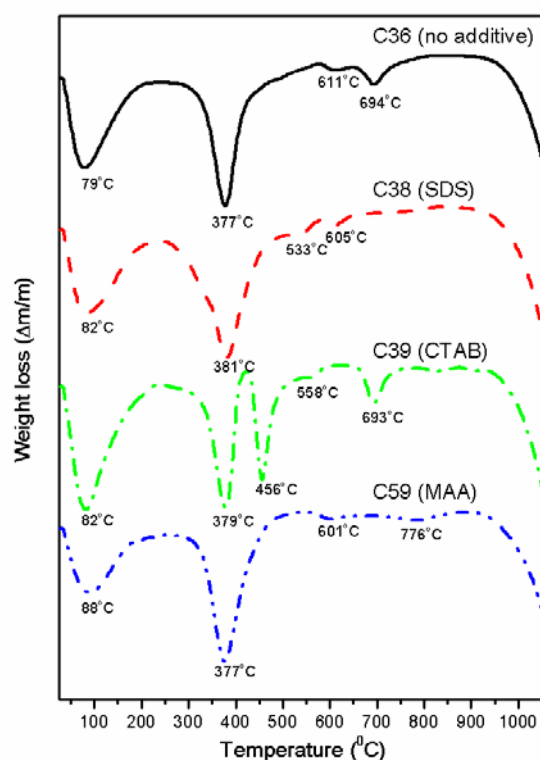


Fig. 1. DTG curves of samples prepared with/without organic reagents.

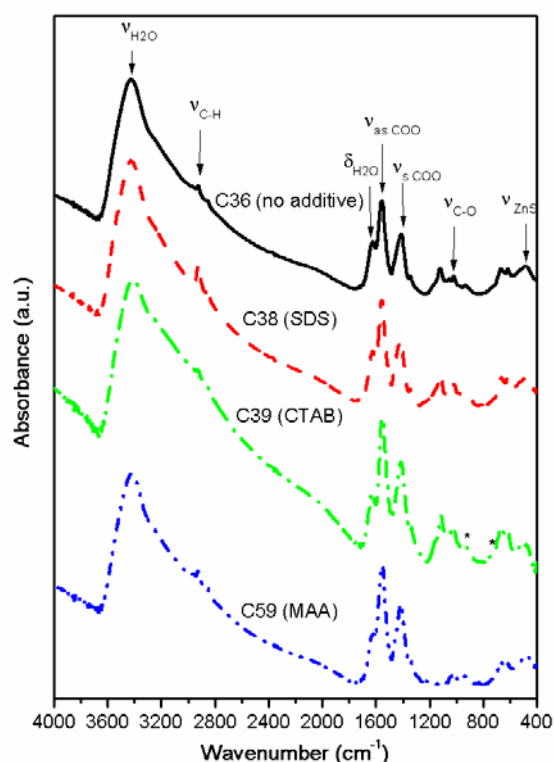


Fig. 2. FT-IR spectra of ZnS:Mn<sup>2+</sup> samples prepared with/without organic reagents.

The organic impurities adsorbed on the surface of ZnS:Mn<sup>2+</sup> particles are put in evidence by the infrared spectroscopy (Fig. 2). Besides the broad and weak band at about 480 cm<sup>-1</sup> assigned to Zn-S bond, FT-IR spectra are dominated by the characteristic absorption bands of water and acetate CH<sub>3</sub>COO<sup>-</sup> ions situated in 1300-1700 cm<sup>-1</sup> range [35]. Contrary to our expectations, FT-IR spectra of ZnS:Mn<sup>2+</sup> samples obtained with SDS (C38), CTAB (C39) and MAA (C59) contain no signals related to the additives. It seems that the amount of the residual organic additive is so small, that their specific vibrations are difficult to observe.

FT-IR and TGA investigations put in evidence the high capacity of ZnS:Mn<sup>2+</sup> powders to absorb especially acetate ions from the precipitation medium, thus illustrating their large surface area in correlation with the small particle dimensions.

### 3.2. Photoluminescence properties

Under ultraviolet excitation, all ZnS:Mn<sup>2+</sup> powders show orange luminescence with variable brightness, function of the synthesis conditions. The emission (PL) spectra of samples prepared without organic additives are depicted in Fig. 3. The un-activated C35 sample exhibits only a weak blue luminescence centred at about 450 nm, attributed to the defect-related emission of the ZnS host. The PL spectra of Mn<sup>2+</sup> doped samples C32-C36 show a second, strong emission band centred around 602 nm that tends to shift toward longer wavelengths with manganese concentration. This characteristic orange emission is associated with <sup>4</sup>T<sub>1</sub>-<sup>6</sup>A<sub>1</sub> electronic transitions inside the manganese ion [36].

Fig. 4 shows the excitation (PLE) spectra for the Mn<sup>2+</sup> characteristic emission band in samples C32-C36 with different doping levels. The maximum excitation peak of Mn<sup>2+</sup> emission centred at about 335 nm is related to the fundamental absorption of the host-lattice (indirect excitation) whereas the relative smaller spectral peaks in the 375-575 nm domain arise from the direct excitation transitions of Mn<sup>2+</sup>. According to the literature, these absorption peaks observed at about 390, 429, 469, 501, and 535 nm are attributed to the transitions between the <sup>6</sup>A<sub>1</sub>(<sup>6</sup>S)

ground state and the excited states of  ${}^4E({}^4D)$ ,  ${}^4T_2({}^4D)$ ,  ${}^4A_1({}^4G)$  and  ${}^4E({}^4G)$ ,  ${}^4T_2({}^4G)$ ,  ${}^4T_1({}^4G)$  within the  $Mn^{2+} 3d^5$  configuration, respectively [23, 36].

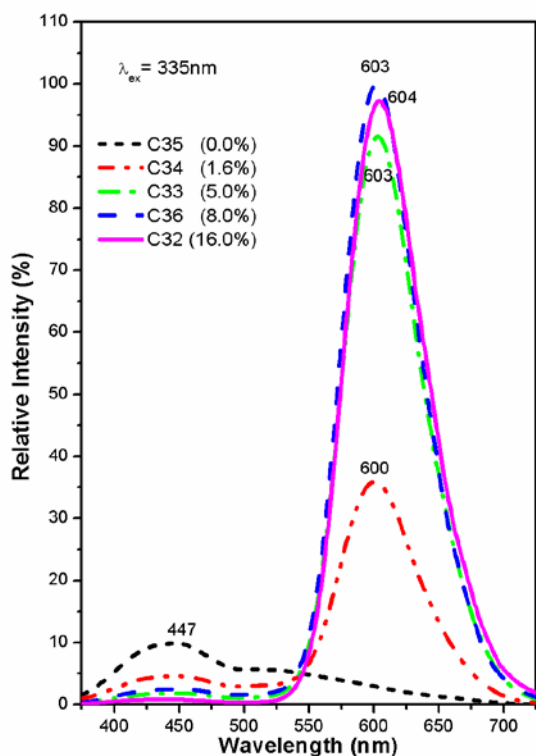


Fig. 3. PL spectra of  $ZnS:Mn^{2+}$  powders prepared with various  $Mn^{2+}$  amounts.

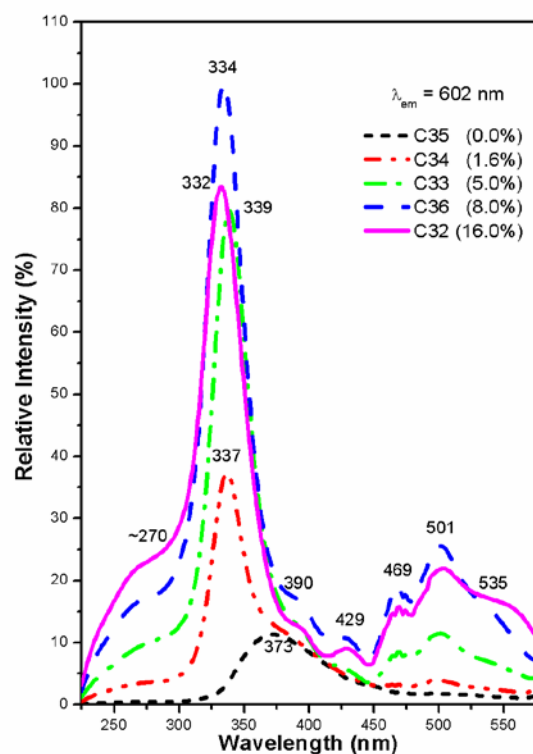


Fig. 4. PLE spectra of  $ZnS:Mn^{2+}$  powders prepared with various  $Mn^{2+}$  amounts.

It seems that the PLE peaks associated with both the host-lattice and Mn-ions are directly related to the Mn doping level that influences their position and intensity. A large MnS amount, incorporated or segregated on particle surface determines a decrease of the fundamental ZnS absorption band centred at about 335 nm.

The relative intensity of the blue and orange emissions is plotted as a function of the actual manganese concentration, as determined by ICP-OES analysis (Fig. 5). The sample without  $Mn^{2+}$  shows only the blue self-activated (SA) luminescence related with the point defects of the ZnS-host. As soon as  $Mn^{2+}$  is incorporated, the intensity of this blue emission decreases and the orange emission comes up, since the energy transfer from ZnS host toward  $Mn^{2+}$  centres is very efficient. The luminescence intensity of the orange band increases in parallel with  $Mn^{2+}$  concentration and then decreases (concentration quenching). The maximum of intensity is reached at about 0.25%  $Mn^{2+}$ , for an optimal ratio between the number of the Mn-emission centres and the quenching ones.

The blue band intensity decreases continuously with the increase of  $Mn^{2+}$  amount, due to the decrease of the numbers of SA centres related with the ZnS lattice defects.

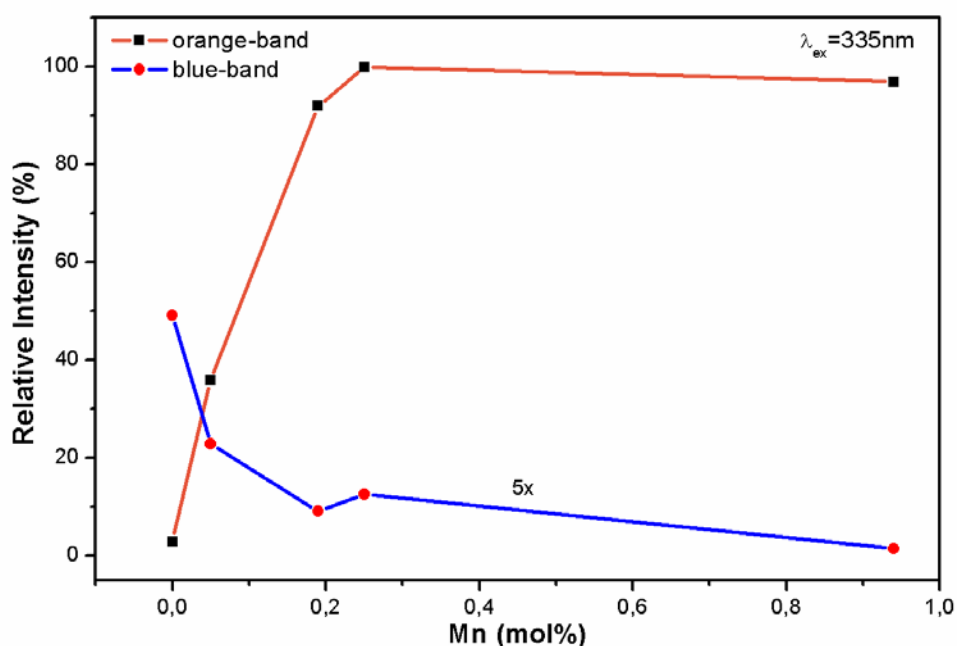


Fig. 5. Relative intensity of the orange and blue bands versus the real Mn concentration in samples prepared with no organic additives.

PL and PLE spectra of  $\text{ZnS:Mn}^{2+}$  powders precipitated from a medium with identical initial Mn-concentration (8.0 mol%) and with various organic additives are depicted in Fig. 6 and Fig. 7, respectively.

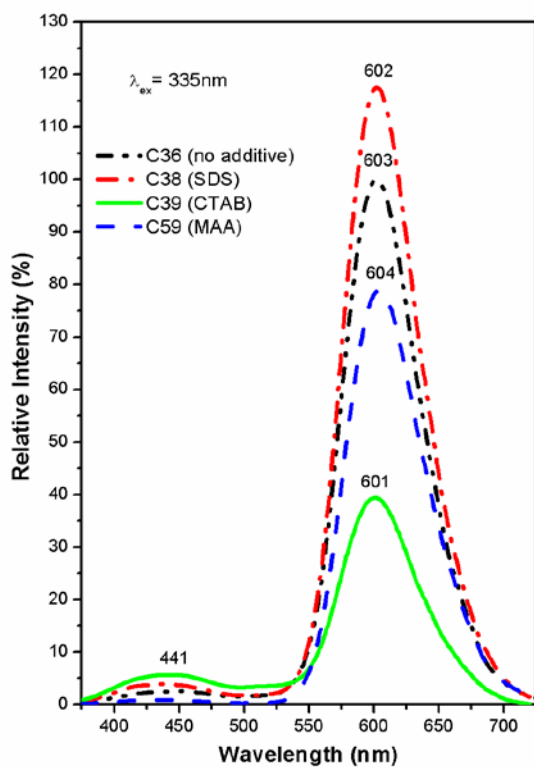


Fig. 6. PL spectra of  $\text{ZnS:Mn}^{2+}$  powders prepared with/without organic additives.

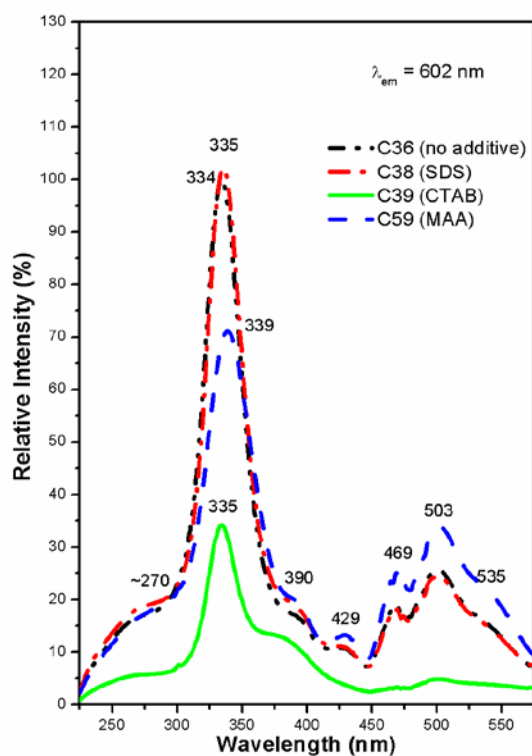


Fig. 7. PLE spectra of  $\text{ZnS:Mn}^{2+}$  powders prepared with/without organic additives.

The addition of SDS increases the intensity of the orange emission with about 20% whereas the MAA and CTAB decreases it with about 20% and 60%, respectively, in comparison with the no-additive sample. This effect could be related mainly with the actual concentration of the Mn-doping into ZnS-crystals i.e. 0.25% (no-additive samples), 0.28% (SDS-sample), 0.74% (MAA-sample) and 0.05% (CTAB-sample). For the MAA-sample, the Mn-concentration quenching effect is accompanied by the MAA quenching action as revealed by our preliminary study [33].

PLE spectra of samples prepared with/without organic additives illustrate the direct and indirect excitation paths in ZnS:Mn<sup>2+</sup> powders. The relative intensity of the PLE peaks associated with the transitions within the Mn<sup>2+</sup> 3d<sup>5</sup> configuration (direct excitation path) is in concordance with the actual Mn doping level as determined by ICP-OES. The position and the intensity of the PLE peaks associated with the ZnS fundamental absorption (indirect excitation path) are strongly influenced by the organic additive. CTAB and especially MAA show a strong diminishing effect on the ZnS host-lattice absorption capability.

PL and PLE spectra suggests that the luminescence performances of ZnS:Mn<sup>2+</sup> samples are determined not only by the amount of Mn<sup>2+</sup> incorporated into the host crystals, but also by the organic additive adsorbed on the surface of particles. One can presume that the adsorbed SDS acts as weak molecular sensitizer whereas the adsorbed MAA and especially CTAB behave as a molecular quencher for Mn-luminescence.

The strong orange photoluminescence of the un-annealed ZnS:Mn<sup>2+</sup> powders obtained in our experimental conditions could be associated with the particle nano-dimension.

### 3.3. Morphological and structural aspects

Fig. 8 shows the transmission electron microscopy (TEM) images of samples obtained with or without organic reagent. They illustrate that ZnS:Mn<sup>2+</sup> powders consist from very small particles with diameters less than 10 nm that, due to their large surface area, show a strong tendency toward agglomeration.

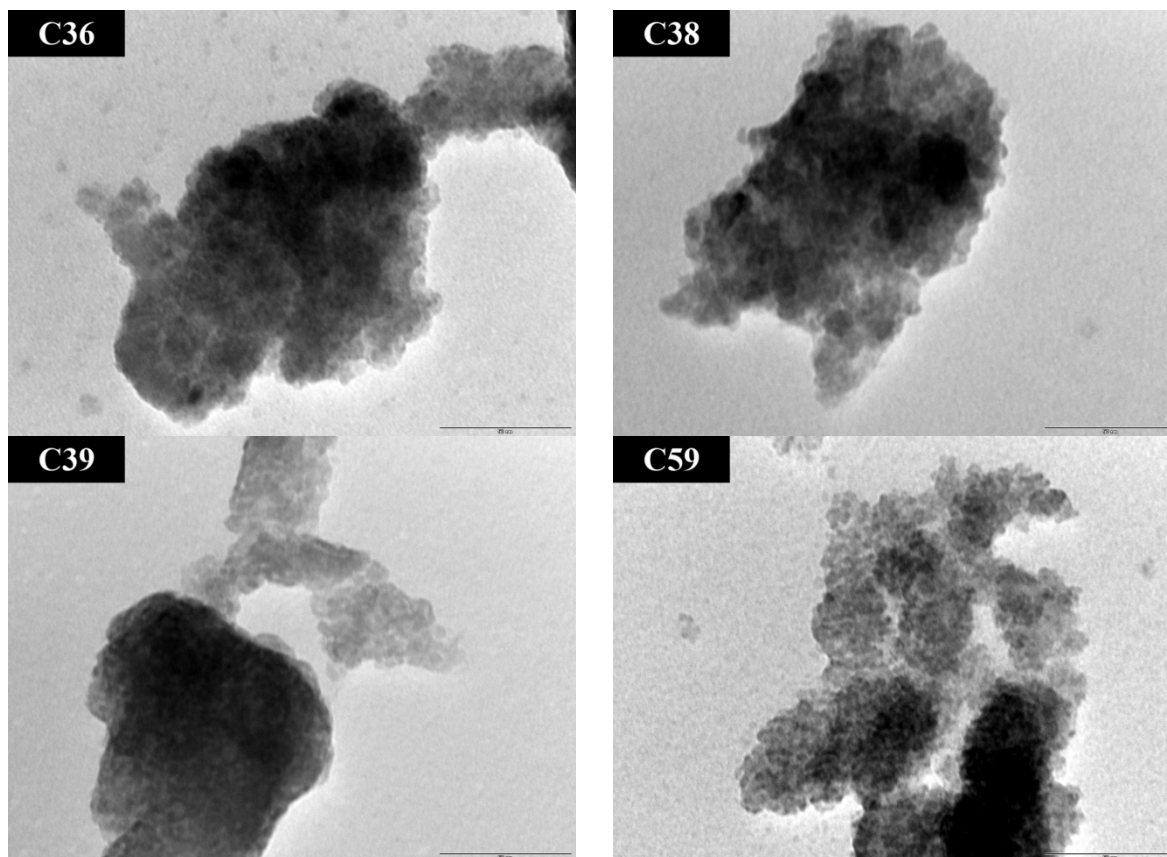


Fig. 8. TEM images of Mn-doped ZnS powders prepared with/without organic additives: C36 (no additive), C38 (SDS), C39 (CTAB), C59 (MAA); scale bar = 50 nm.

XRD patterns of ZnS were interpreted using the JAVA based software namely Materials Analysis Using Diffraction (MAUD) [37] whereas the unit cell parameters were calculated by Rietveld refinement, using the POWDERCELL software [38]. They indicate the formation of a single phase, nanocrystalline material with pure ZnS cubic structure, whatever the synthesis conditions.

Fig. 9 illustrates the three specific diffraction peaks originating from (111), (220) and (311) planes of the zinc blende structure (PDF 65-0309).

Relevant information was provided by the microstructural parameters obtained from X-ray profile Fourier analysis (Table 2). In this respect, the (111), (220) and (311) diffraction profiles, at  $2\Theta = 28.54$ ;  $47.46$  and  $56.32$  degrees, respectively, were analysed by Warren-Averbach method [39, 40]. The analysis was performed for ZnS-cubic system (PDF 65-0309; G.S. 216; unit cell parameters:  $a=b=c=0.540$  nm;  $V=0.1574$  nm<sup>3</sup>).

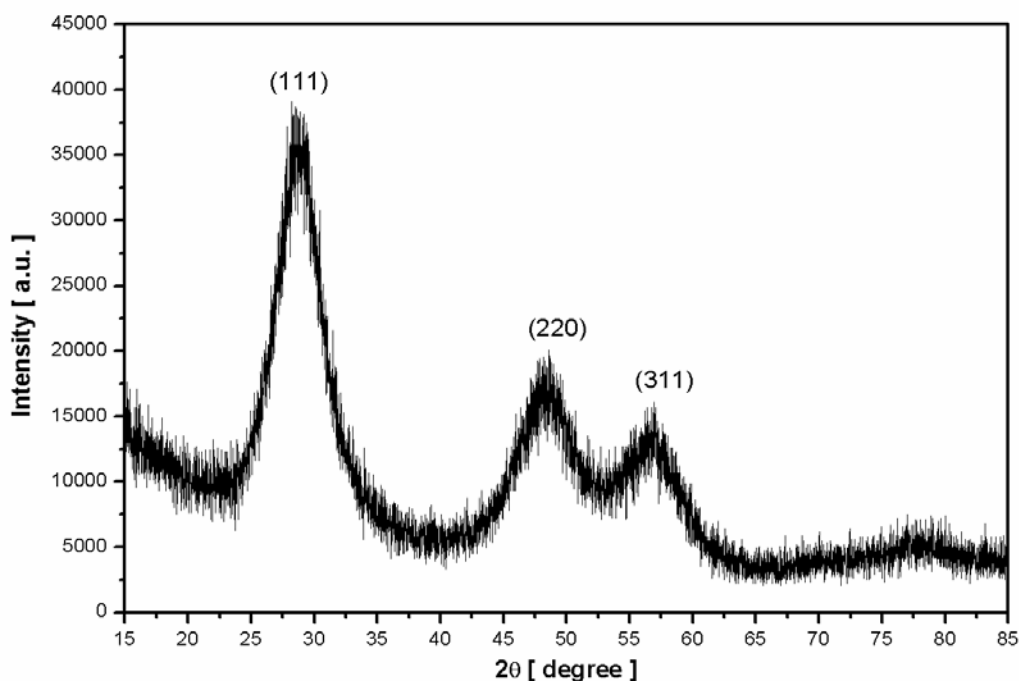


Fig. 9. XRD pattern of un-doped ZnS sample (C35).

The microstructural parameters i.e. the effective crystallite mean size ( $D_{\text{eff}}$ ) and the root mean square (r.m.s.) of the micro-strains  $\langle \varepsilon^2 \rangle^{1/2}$  hkl averaged along the [hkl] direction were determined from the XRD profile lines processed by XRLINE program [41].

Table 2. Unit cell parameters of some ZnS:Mn<sup>2+</sup> powders and their relevant characteristics

Samples	Synthesis details		PL	Structural data			
	Organic additive	Mn conc. [mol%]	Intensity [%]	a=b=c [nm]	V [nm <sup>3</sup> ]	$D_{\text{eff}}$ [nm]	$\langle \varepsilon^2 \rangle^{1/2} \times 10^2$
C32	-	0.94	97	0.5422	0.1590	3.0	0.9584
C35	-	0.00	3	0.5416	0.1588	3.0	0.9455
C36	-	0.25	100	0.5413	0.1587	3.0	0.9456
C38	SDS	0.28	118	0.5422	0.1594	3.0	0.9520
C39	CTAB	0.05	39	0.5417	0.1589	3.1	1.0102
C59	MAA	0.74	79	0.5413	0.1586	3.0	0.9455

All ZnS-based powders are built-up from very small nanocrystals (3.0-3.1 nm), with a micro-strain density of a medium value (r.m.s. = 0.00095-0.0010). This particle nano-dimension accounts for the strong orange photoluminescence in relation with the PL confinement effect.

The microstructural parameters seem to be dependent of both the Mn-concentration and organic additive.

The particles dimension and micro-strain probability of C59 and C38 powders, obtained with MAA and SDS, respectively, seem not to be influenced by the organic additive, as compared with the no-additive C36 powder ( $D_{\text{eff}} \sim 3.0$  nm). Instead, the CTAB cationic surfactant tends to increase both the packing micro-strain density and particle dimension ( $D_{\text{eff}} \sim 3.1$  nm).

On the other hand, the unit cell volume and the micro-strain probability tend to increase with Mn-concentration, in accordance with the ions radii i.e. 0.074 nm for  $\text{Zn}^{2+}$  and 0.080 nm for  $\text{Mn}^{2+}$ , in tetrahedral coordination. The non-monotonous increase of the unit cell volume with the actual activator amount can be explained by the fact that, part of the manganese is deposited as MnS on particle surface, and not inside the crystal.

#### 4. Conclusions

Manganese-doped zinc sulphide nanocrystalline powders were obtained by WCS-SimAdd route that allows a good control of the precipitation parameters i.e. medium pH, cation and anion concentration etc. The careful choice of the precipitation conditions i.e. optimal ratio between manganese and zinc ions, adequate composition of the medium (solvent, organic additive, pH), accurate reagent flow and volume ratios, etc., enabled us to obtain homogeneous and strong orange emitting  $\text{ZnS:Mn}^{2+}$  nanocrystals.

The organic additives, either passivating agent or anionic/cationic surfactant, show similar effect on morpho-structural properties of  $\text{ZnS:Mn}^{2+}$  powders, but they exhibit different impact on PL performances, in relation with their strong influence on the actual Mn concentration (0.6-9.3% co-precipitation level). TEM and XRD investigations indicate the formation of single phase/cubic  $\text{ZnS:Mn}^{2+}$  powders with crystallites of about 3 nm.

The highest PL performances are observed for  $\text{ZnS:Mn}^{2+}$  nanocrystalline powders precipitated at room temperature, in methanol-based medium with SDS as additive, from sodium sulphide and Zn-Mn acetate mixture containing 8 mol% Mn.

The strong orange photoluminescence of the  $\text{ZnS:Mn}^{2+}$  powders obtained in our experimental conditions can be associated with the particle nano-dimension illustrated by both XRD and TEM investigations, and the consequent PL confinement.

#### Acknowledgments

This work was supported by CNCSIS – UEFISCSU, project number PNII – IDEI 2488/2008.

#### References

- [1] M. Dhanam, B. Kavitha, Neethajose, D.P. Devasia, *Chalcogenide Lett.* **6**, 713 (2009).
- [2] J.S. Jie, W.J. Zhang, I. Bello, C.S. Lee, S.T. Lee, *Nano Today* **5**, 313 (2010).
- [3] D. Bera, L. Qian, T.K. Tseng, P.H. Holloway, *Materials* **3**, 2260 (2010).
- [4] X.S. Fang, T.Y. Zhai, U.K. Gautam, L. Li, L.M. Wu, Y. Bando, D. Golberg, *Prog. Mater. Sci.* **56**, 175 (2011).
- [5] X.J. Zheng, Y.Q. Chen, T. Zhang, C.B. Jiang, B. Yang, B. Yuan, S.X. Mao, W. Li, *Scr. Mater.* **62**, 520 (2010).
- [6] H.R. Pouretedal, A. Norozi, M.H. Keshavarz, A. Semnani, *J. Hazard. Mater.* **162**, 674 (2009).
- [7] M.E. Mathew, J.C. Mohan, K. Manzoor, S.V. Nair, H. Tamura, R. Jayakumar, *Carbohydr. Polym.* **80**, 443 (2010).
- [8] E. Mohagheghpour, M. Rabiee, F. Moztarzadeh, M. Tahriri, M. Jafarbeglou, D. Bizari, H. Eslami, *Mater. Sci. Eng., C* **29**, 1842 (2009).

- [9] P. Thiyagarajan, M. Kottaisamy, M.S.R. Rao, *J. Lumin.* **129**, 991 (2009).
- [10] S. Srivastava, R.K. Srivastava, S.G. Prakash, *Dig. J. Nanomater. Biostruct.* **5**, 829 (2010).
- [11] R.N. Bhargava, D. Gallagher, X. Hong, A. Nurmikko, *Phys. Rev. Lett.* **72**, 416 (1994).
- [12] A.A. Bol, A. Meijerink, *J. Lumin.* **87-89**, 315 (2000).
- [13] M. Dhanam, D.P. Devasia, B. Kavitha, B. Maheswari, *Dig. J. Nanomater. Biostruct.* **5**, 379 (2010).
- [14] M. Navaneethan, J. Archana, K.D. Nisha, Y. Hayakawa, S. Ponnusamy, C. Muthamizhchelvan, *J. Alloys Compd.* **506**, 249 (2010).
- [15] Q.Z. Yao, G. Jina, G.T. Zhou, *Mater. Chem. Phys.* **109**, 164 (2008).
- [16] C. Bi, L.Q. Pan, M. Xu, J.H. Yin, L.Q. Qin, J.M. Liu, H. Zhu, J.Q. Xiao, *Mater. Chem. Phys.* **116**, 363 (2009).
- [17] A.P. Gondikas, E.K. Jang, H. Hsu-Kim, *J. Colloid Interface Sci.* **347**, 167 (2010).
- [18] S.K. Mehta, S. Kumar, *J. Lumin.* **130**, 2377 (2010).
- [19] Y. Zhang, X.H. Liang, L.C. Li, *Mater. Lett.* **64**, 1521 (2010).
- [20] M. Sharma, S. Kumara, O.P. Pandey, *Dig. J. Nanomater. Biostruct.* **3**, 189 (2008).
- [21] Q.S. Huang, L. Li, J.P. Xu, X.S. Zhang, G.F. Zhang, R.W. Xuan, *Optoelectron. Lett.* **6**, 161 (2010).
- [22] G. Murugadoss, B. Rajamannan, V. Ramasamy, *Digest Journal of Nanomaterials and Biostructures* **5**, 339 (2010).
- [23] W.Q. Peng, S.C. Qu, G.W. Cong, X.Q. Zhang, Z.G. Wang, *J. Cryst. Growth.* **282**, 179 (2005).
- [24] Z.L. Wang, Y. Liu, Z. Zhang, *Handbook of nanophase and nanostructured materials synthesis*, Tsinghua University Press and Kluwer Academic Plenum Publishers, New York (2002).
- [25] A.-I. Cadis, E.-J. Popovici, E. Bica, I. Perhaita, L. Barbu-Tudoran, E. Indrea, *Chalcogenide Lett.* **7**, 631 (2010).
- [26] L. Muresan, E.-J. Popovici, R. Grecu, L. Barbu Tudoran, *J. Alloys Compd.* **471**, 421 (2009).
- [27] E.-J. Popovici, M. Stefan, F.I. Lucaci, L. Muresan, E. Bica, M. Morar, E. Indrea, L. Barbu-Tudoran, *Phys. Proc.* **2**, 603 (2009).
- [28] E.-J. Popovici, M. Morar, L. Mureşan, R. Grecu, L. Barbu-Tudorana, E. Indrea, *J. Optoelectron. Adv. Mater. - Symposia* **1**, 1000 (2009).
- [29] A.-R. Tomsa, E.-J. Popovici, A.-I. Cadis, M. Stefan, L. Barbu-Tudoran, S. Astilean, *J. Optoelectron. Adv. Mater.* **10**, 2342 (2008).
- [30] M. Ladar, E.-J. Popovici, I. Baldea, R. Grecu and E. Indrea, *J. Alloys Compd.* **434-435**, 697 (2007).
- [31] A.-I. Cadis, A.-R. Tomsa, M. Stefan, R. Grecu, L. Barbu-Tudoran, L. Silaghi-Dumitrescu, E.-J. Popovici, *J. Optoelectron. Adv. Mater. - Symposia* **2**, 111 (2010).
- [32] A.-I. Cadis, E.-J. Popovici, E. Bica, L. Barbu-Tudoran, *Stud. Univ. Babes-Bolyai Chem.* **55**, 265 (2010).
- [33] A.-I. Cadis, E.-J. Popovici, E. Bica, I. Perhaita, L. Barbu-Tudoran, E. Indrea, *CAS: 2010 Int. Semicond. Conf. Proc.*, 513 (2010).
- [34] J. G. Speight, *Lange's Handbook of Chemistry*, 16<sup>th</sup> ed., McGraw-Hill: New York (2005).
- [35] B.H. Stuart, *Infrared Spectroscopy: Fundamentals and Applications*, John Wiley & Sons Ltd., Chichester (2004).
- [36] R. Kripal, A.K. Gupta, S.K. Mishra, R.K. Srivastava, A.C. Pandey, S.G. Prakash, *Spectrochim. Acta, Part A* **76**, 523 (2010).
- [37] L. Lutterotti, S. Gialanella, *Acta Mater.* **46**, 101 (1998).
- [38] W. Kraus, G. Nolze, *J. Appl. Crystallogr.* **29**, 301 (1996).
- [39] J.G.M. van Bercum, A.C. Vermeulen, R. Delhez, T.H. de Keijser, E.M. Mittemeijer, *J. Appl. Crystallogr.* **27**, 345 (1996).
- [40] E. Indrea, A. Barbu, *Appl. Surf. Sci.* **106**, 498 (1996).
- [41] N. Aldea, E. Indrea, *Comput. Phys. Commun.* **60**, 155 (1990).